Journal of Building Engineering 70 (2023) 106286

Contents lists available at ScienceDirect

Journal of Building Engineering

journal homepage: www.elsevier.com/locate/jobe

A new Coplanar Dual Core Buckling-Restrained Brace

X. Cahís [a,*], A. Catalan [b], A. Benavent-Climent [c], D. Trias [a,1]

[a] Department of Mechanical and Construction Engineering, University of Girona, Girona, Spain
[b] Department of Construction, University of Oviedo, Gijón, Spain
[c] Department of Mechanical Engineering, Technical University of Madrid, Madrid, Spain

ARTICLE INFO

Keywords:
All-steel buckling-restrained brace
Hysteresis damper
Energy dissipation
Low-cycle fatigue
High-mode buckling

ABSTRACT

This study presents a new all-steel Buckling-Restrained Brace (BRB) named Coplanar Dual Core (CDC) BRB, that consists of a rectangular cross-sectional core divided into two coplanar yielding lateral bands, whose movements are constrained by an external restrainer (ER) and by an internal restrainer (IR). In contrast with the traditional BRB with dog-bone shaped core, the CDC-BRB has the advantage that the core can be easily extracted and inspected. The ER is composed of two rectangular tubes welded to a pair of rectangular solid calibrated bars. The core and IR are simultaneously laser cut from the same sheet of steel, which provides additional advantages: minimum material waste, minimum laser cut length, regular and well controlled gap, reduction of weight and manufacturing cost. Formulae to design the CDC-BRB, to determine the appropriate values of the gaps, and to predict its response and ultimate energy dissipation capacity are proposed. Four specimens representing the new CDC-BRBs with different gaps are tested under cyclic loadings to failure. The results of the tests show that the cyclic behavior of the new CDC-BRB is stable, highly dissipative, and its response and ultimate energy dissipation capacity can be well predicted insofar the gaps fit the proposed values.

1. Introduction

Buckling Restraining Braces (BRBs) are designed to lend lateral deformation and damage control to seismic-resistant structures by energy dissipation through plastic deformation. This deformation is concentrated in a slender steel core that must resist multiple reversal axial forces. The stability of the core in compression is achieved by embedding it in a stiffer buckling-restraining element, which is conventionally a steel tube filled with mortar or concrete [1–3]. The BRBs' restrainer must provide a gap for the core to expand in compression, which would ripple in high-mode buckling. The wider is the gap, the wider are the core waves' amplitudes and the higher are their outward forces against the restrainer, and the consequent friction forces [4–7]. The transfer of forces to the restrainer in compression reduces both the symmetry of the hysteretic loops and the strain uniformity along the core [8]. Conventional BRB braces reduce this friction force by wrapping the core in a low-friction debonding layer before the mortar is cast on the restraining steel tube [9–12].

To eliminate the fabrication steps associated with pouring and curing the mortar or concrete, the BRB can be made entirely of steel, thus called all-steel BRBs. Even though all-steel BRBs could offer several advantages when compared to conventional BRBs —weight reduction, lower manufacturing costs, and the possibility of core inspection [5,13–15]— they can only achieve comparable ductility and energy dissipation capacity if provided with a tight, regular core-to-restrainer gap, which is difficult to ensure in practice [15]. In fact, the regularity and the size of both the in-plane and the out-of-plane gaps are key aspects for the design of all-steel BRBs. Gaps larger than

* Corresponding author.
E-mail address: xavier.cahis@udg.edu (X. Cahís).
[1] Serra Hunter Fellow.

https://doi.org/10.1016/j.jobe.2023.106286
Received 19 January 2023; Received in revised form 28 February 2023; Accepted 11 March 2023
Available online 20 March 2023

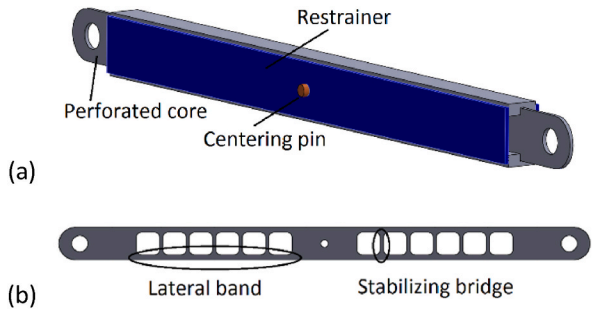

Fig. 1. Perforated Core Buckling-Restrained Brace (PC-BRB): (a) assembled PC-BRB; (b) detail of the core.

required would increase the normal thrust on the restrainers and, consequently, the friction forces. Gaps smaller than required prevent the core from freely expanding and would cause grip. The authors developed in past studies [16] an all-steel BRB, named Perforated Core Buckling Restrained Brace (PC-BRB) whose core is split into two yielding lateral bands connected by stabilizing bridges (Fig. 1).

In the PC-BRB, the in-plane and out-of-plane gaps are formed by milling longitudinal deep grooves along solid rectangular bars to guide and stabilize the yielding lateral bands of the core in compression. While the PC-BRB showed a satisfactory performance in the tests and its behavior and ultimate energy dissipation capacity can be easily predicted, there is room for improvement. First, an expensive milling manufacturing process is required to guarantee the regularity and size of the grooves along the solid rectangular bars. Second, because the in-plane buckling stabilizing bridges provide discontinuous bracing, they produce inherent bending in the lateral bands and a loss of effective yielding length. Third, the restrainer member of the PC-BRB is heavy. In this work a new all-steel BRB, named Coplanar Dual Core Buckling-Restrained Brace (CDC-BRB) is proposed to resolve these issues (Fig. 2). In the new CDC-

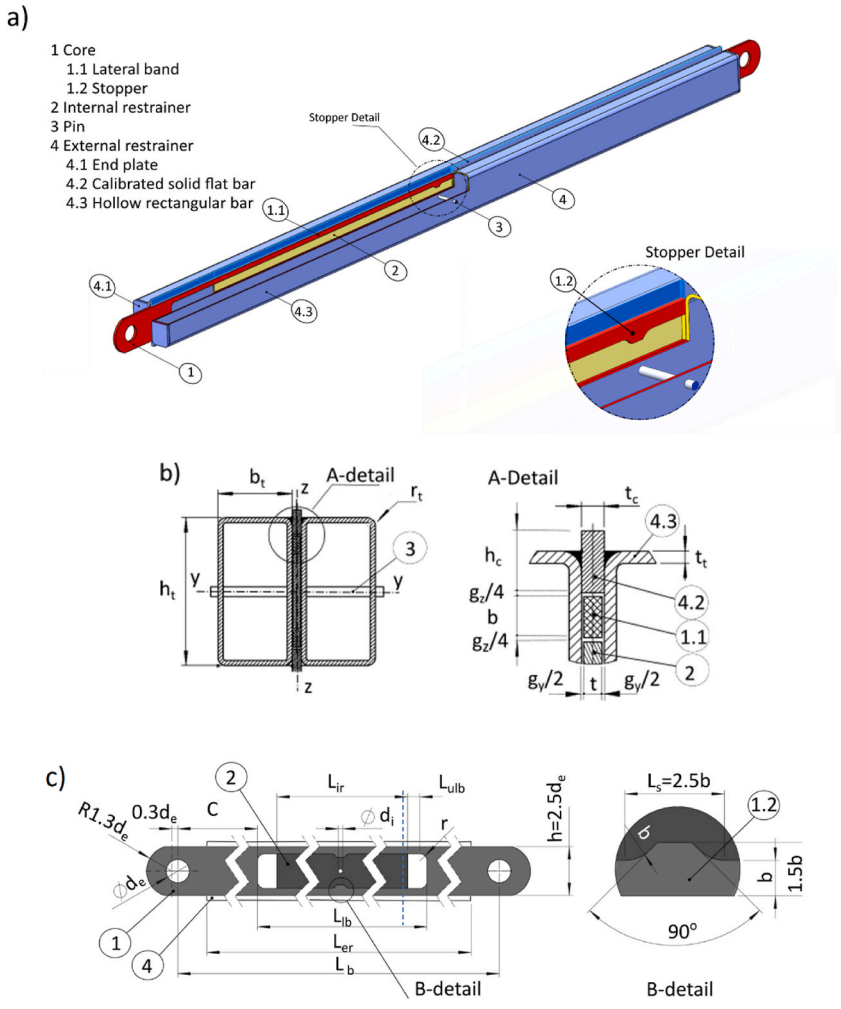

Fig. 2. SC-BRB assembly and geometry of parts: a) Parts' assembly; b) Brace cross-section; c) Core and internal core, with geometric detail of the stopper.

BRB, the stabilizing bridges are replaced by a continuous steel plate, which ensures continuous restraining of the lateral bands while preventing their inherent bending, thereby increasing their effective yielding length. Moreover, both the weight and the manufacturing costs of the restrainer are significantly reduced. It is worth noting that the laser cut and component processing of CDC-BRB is not an extra cost; it replaces the more cumbersome cutting process of the PC-BRB while reducing manufacturing time and material waste.

In sum, the motivation of this research is improving the existing all-steel BRBs in the following aspects. First, to simplify the manufacturing process of the BRB while ensuring that the gaps between the core and the restrainers are regular and tightly adjusted to the required values. Second, to facilitate the extraction and inspection of the core after a severe seismic event. Third, to reduce the cost of manufacturing the core of the BRB through reducing the required length of laser cuts. Fourth, to avoid/minimize the waste of material. Fifth, to achieve a BRB with highly predictable behavior in terms of low-cycle fatigue life. Sixth, to reduce the weight of the BRB. One of the main novelties of the new BRB is that the core and the interior restrainer are simultaneously laser cut from the same sheet of steel, which provides minimum material waste, minimum laser cut length, regular and well controlled gap, and reduction of weight and manufacturing cost. This study adds to the knowledge base on BRBs' new formulae to design the device, to determine the appropriate values of the gaps, to predict its response and ultimate energy dissipation capacity, and to prevent the local buckling of the unrestrained end parts of the core. This study explains how the CDC-BRB should be designed and manufactured to attain a predictable response and high energy dissipation capacity. Attention is paid to the size of the core-to-restrainer gaps, and a design value is proposed. Moreover, the study presents the results of an experimental campaign highlighting the good performance of the CDC-BRB and the importance of setting the core-to-restrainer gaps at the proposed values.

2. Concept, geometry, and manufacturing

Fig. 2 shows the new CDC-BRB. It comprises a core, restrainers and a pin. The core has a yielding zone consisting of two lateral bands (referred to as "yielding lateral bands" herein) whose buckling is prevented by the External and the Internal Restrainers (ER and IR, respectively). The yielding lateral bands have a ridge at mid length (Fig. 2c, B-detail) that indents into the IR and serves as stopper to prevent relative movements between the yielding lateral bands and the IR along the axis of the CDC-BRB. The ER stays centered on the core and on the IR owing to the presence of an internal pin which, if pulled out, would permit core extraction and inspection. The ER is made up of two rectangular tubes with end plates, welded at opposite sides of two calibrated rectangular bars of width t_c, leaving room for the core to expand under compressive loads.

The total in-plane and out-of-plane gaps of the lateral bands are g_Z and g_Y (see detail A in Fig. 2b). The gaps' values are a crucial issue in the design of the CDC-BRB. In past studies [8], the authors found that the outermost part of the yielding lateral bands can undergo residual negative strains up to 13%. Based on these results, here it is proposed to set g_Y, g_Z at the following values:

$$g_Y = 0.13\nu t \;\; ; \;\; g_Z = 0.26\nu b \tag{1}$$

where ν is the Poisson ratio ($\nu = 0.5$ in plastic deformation), t is the thickness, and b the width of the yielding lateral bands, as shown in Fig. 2b. Fig. 3a depicts the connection of the CDC-BRB to the frame, while Fig. 3b shows the maximum distance between the gussets and the ER to allow the maximum amplitude deformation demanded by the ASCI qualifying test [17]. Therefore, to prevent the contact between the ERs and the gussets in the distance, C_o must satisfy:

$$C_O \geq 1.6\, d_e + \xi\delta_{Ed} \tag{2}$$

where, d_e is the diameter of the connection pin; ξ is a dimensionless factor that need to account for occasional unbalanced deformation of the yielding lateral bands on maximum deformation, and must be taken $\xi \geq 1$. Based on the experimental results of the two specimens manufactured according to Eq. (1), we propose $\xi = 1.1$. In turn, δ_{Ed} is the elongation of the BRB at the design interstory drift ID_{Ed} given by:

$$\delta_{Ed} = ID_{Ed}\, cos\, \phi \tag{3}$$

where ϕ is the angle of the BRB axis with respect to the horizontal.

The distance C (Fig. 3b) must be long enough to guide the core inside the ER so that the axial load eccentricity $e_{g,Z}$ is kept under

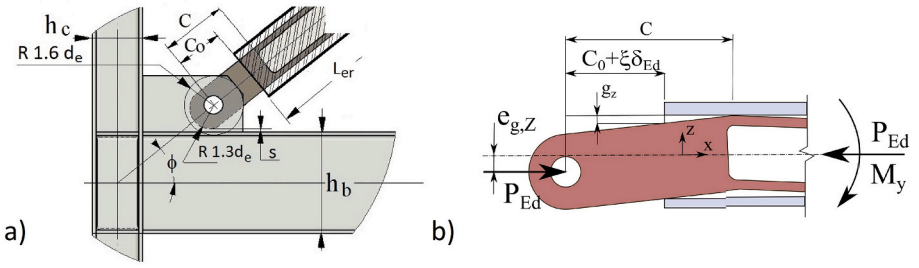

Fig. 3. a) Brace-to-frame connection; b) One end's core at maximum elongation.

control; it is proposed to adopt:

$$C = 2(C_0 + \xi\delta_{Ed}) \tag{4}$$

To avoid the strain concentration effect [8] at the ends of the yielding lateral bands of the core, and for the sake of simplicity, it is proposed to make $r = b$ (see Fig. 2c). To prevent the lateral band ends from buckling, one may adopt:

$$L_{ulb} \leq 0,5L_{w,z} \tag{5}$$

Here L_{ulb} is the distance shown in Fig. 2c, and $L_{w,z}$ is the high-mode buckling length determined from Eq. (6) [4,8]:

$$L_{w,z} = 0.861\ \varepsilon_a^{-0.631} b \tag{6}$$

where b is the width of the yielding lateral bands as shown in Fig. 2b, ε_a is the maximum strain amplitude, which can be taken as two times the maximum compressive strain ε_c calculated with:

$$\varepsilon_c \cong IDR \frac{\sin 2\phi}{2} \frac{L_{wp}}{L_y} \tag{7}$$

Here, IDR is the interstory drift ratio, L_y is the length of the yielding lateral bands of the core with constant cross-sectional area, and $L_{wp} = \sqrt{H^2 + L^2}$ is the work-point to work-point length, where H is the story height and L the span of the bay when diagonal concentric bracing is considered.

To optimize the manufacturing process, several units would ideally be cut from the same sheet of steel, as shown in Fig. 4a. Laser cut is recommended. It is also recommended to include micro-connectors between the lateral bands and the IR (see Fig. 4b) to enhance the uniformity of the cross-sectional area of the yielding lateral bands, plus a straight cut —by reducing thermal deformations— during the cutting process, while keeping the IR in the exact position during the assemblage of the CDC-BRB. The contribution of the micro-connectors to the mechanical properties of the CDC-BRB is negligible, since their width is very small (<1 mm) and will break under very small axial forces.

3. Experimental tests and analysis of the response

3.1. Specimens' characteristics and material properties

Four specimens representing the new CDC-BRB were designed as explained in section 2 and based on the formulae of Annex A (see Table 1). Besides the material properties of the core and the technique used to cut the core and the IR, the main difference among the specimens was the dimension of the gaps g_Y and g_Z. The 2nd and 3rd specimens had the required gaps g_Y and g_Z proposed with Eq. (1). In the 1st specimen, g_Y and $g_Z$were intentionally made much larger than the required values. In the 4th specimen, g_Z was made slightly smaller than the value prescribed by Eq. (1). The purpose was to investigate the influence of the dimensions of the gap on the response of the CDC-BRB. The only difference between the 2nd and 3rd specimens is that in the former, the core, the IR and the ER were new (not reused), whereas in the 3rd specimen the ER of the 2nd specimen was reused. This was done to investigate the extent to which repairing the CDC-BRB —by replacing the core and the IR— could affect its behavior. The strength and length of the specimens were determined by laboratory constraints, i.e. the capacity of the loading servo-controlled hydraulic system and the available column-to-brace testing set-up. The core and the IR of each specimen were CAD-CAM plasma/laser cut from three different steel sheets. Material properties of the specimens' core (Table 2) were determined by a tensile test [19], while we considered normalized properties for the remaining specimen components, manufactured with steel class S275 [20]. In Table 2, F_y and F_u are the yield and ultimate stress of the steel, ω' is the ratio F_u/F_y, and ε_y, ε_u are the yield and ultimate strain of the steel.

The size of the gaps required by Eq. (1) are $g_Y = 0.65$ mm and $g_Z = 2.6$ mm. Table 3 gives the dimensions of the IR and ER components, plotted in Fig. 2. As seen, all specimens shared identical restrainer geometries, except for the size of the gaps g_y and g_z.

Fig. 5 shows how the manufacturing process influenced the uniformity of the cross-section area of the yielding lateral bands of the core through its length. The 1st specimen was plasma cut and showed lower uniformity than the rest of the specimens, being laser cut. The 2nd and 3rd specimens had micro-connectors and exhibit the highest uniformity.

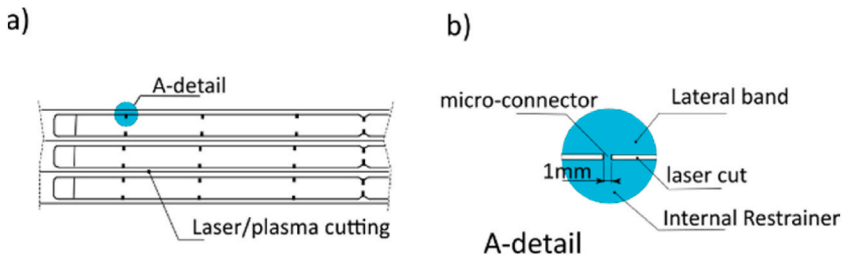

Fig. 4. Core and IR manufacturing: a) cutting layout, b) micro-connector detail.

Table 1
Geometric parameters of the specimens' cores (mm).

Spec	L_b	h	L_{lb}	L_y[a]	b[b]	d_e	r	t	cut	micro-connector
1st	3533	137.5	2792	2702	19.6	55	20	9.84	plasma	no
2nd	3533	137.5	2792	2702	19.5	55	20	10	laser	yes
3rd	3533	137.5	2792	2702	19.56	55	20	10	laser	yes
4th	3533	137.5	2792	2702	19.7	55	20	10	laser	no

[a] L_y is the yielding length, or length of the lateral band with uniform cross-sectional area.
[b] Average value.

Table 2
Cores' steel grades [19] and steel mechanical properties.

Spec	Steel grade [20]	F_y (MPa)	F_u (MPa)	ω'	ε_y	ε_u
1st	S275	323	473	1.43	0.161%	17%
2nd, 3rd	S235	289	443	1.53	0.125%	22%
4th	S235	238	308	1.29	0.112%	15%

F_y = yielding stress, F_u = ultimate stress, $\omega' = F_u/F_y$, ε_y = yielding strain, ε_u = ultimate strain.

Table 3
Geometric parameters of the restraining members (mm).

Spec	L_{ir}	L_{er}	d_i	t_c	h_c	b_t	h_t	r_t	t_t	g_Y	g_Z
1st	2663	3162.5	12	12	25	80	160	8	5	2	4
2nd, 3rd	2663	3162.5	12	10	25	80	160	8	5	0.7	2.6
4th	2663	3162.5	12	10	25	80	160	8	5	0.7	2

3.2. Test set-up, instrumentation, and loading test protocol

The four CDC-BRB specimens were tested with the column-to-BRB subassembly illustrated in Fig. 6a–b. The top specimen's end was pinned to the column, and the joint was also connected to the servo-controlled loading hydraulic jack by two double-pinned struts. The bottom ends of the column and the CDC-BRB specimen were likewise pinned to the strong floor. The angle between the brace and the strong floor was $\phi = 40°$. The instrumentation measured the horizontal load applied by the hydraulic jack, the horizontal piston displacement, total axial deformation of the yielding lateral bands of the core (displacement transducer DT-1 in Fig. 6c), and the partial axial deformations of the lowermost and uppermost parts of the yielding lateral bands of the core (displacement transducers DT-2 and DT-3, respectively, in Fig. 6c). The AISC-341 [17] and EN-15129 [21] load testing protocols shown in Fig. 7 were used, considering a design interstory drift ratio IDR_{Ed} of 1% and a story height of $H = 3$ m, giving a BRB design deformation $\delta_{Ed} = 23$ mm. Under the AISC-314 protocol, the cycles of amplitude of $1.5\delta_{Ed}$ were continuously applied until the failure of the specimen. According to the EN-15129 protocol, after reaching the cycle of amplitude $1.5\delta_{Ed}$, the pattern of loading was repeated starting with the cycles of amplitude $0.25\delta_{Ed}$, until the specimen failed. The 1st, 2nd and 3rd specimens were subjected to the AISC-341 protocol, whereas the 4th specimen was subjected to protocol EN-15129.

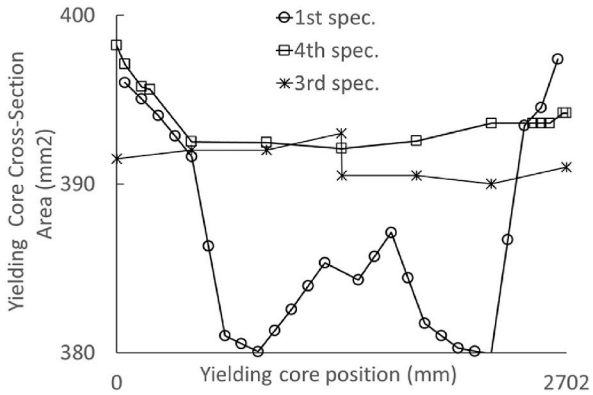

Fig. 5. Distribution of the cross-sectional areal of lateral bands across the yielding lateral bands of the core.

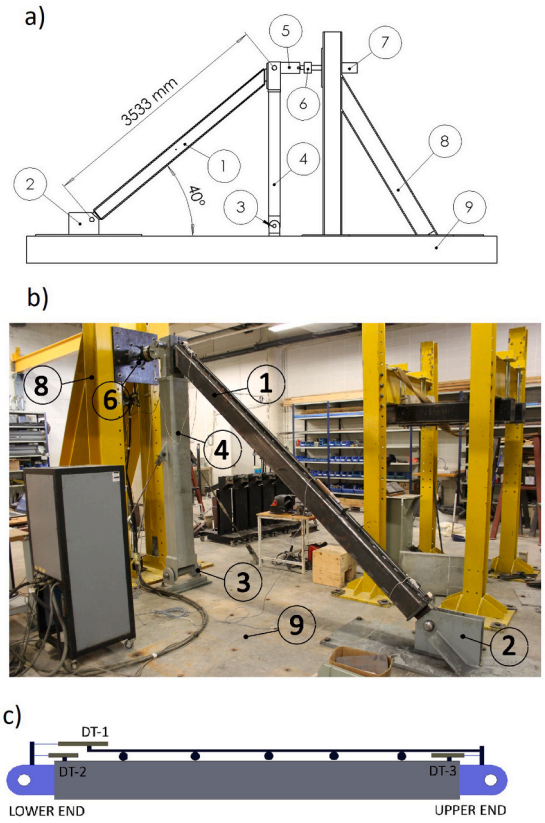

Fig. 6. Test set-up. a) Loading system scheme: 1 CDC-BRB specimen, 2 lower brace connection, 3 lower column connection, 4 double-pinned column, 5 double-pinned struts, 6 load cell, 7 servo-controlled hydraulic jack, 8 reaction frame, 9 strong floor. b) photo of the tests set-up; (c) Specimen instrumentation with displacement transducers.

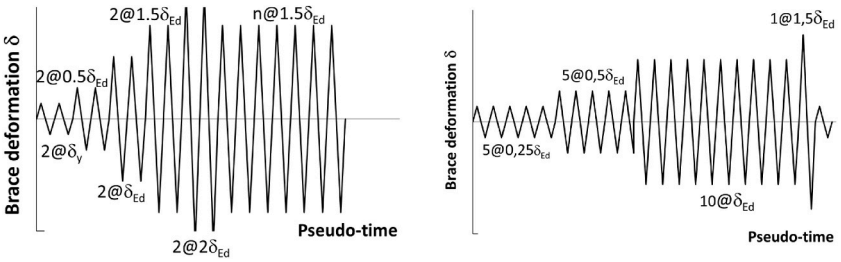

Fig. 7. Test loading protocols: a) AISC-341 [17], b) EN-15129 [21].

3.3. Experimental results and discussion

3.3.1. Global response

Fig. 8 depicts the axial force P versus the axial displacement δ between the ends (i.e. pin connections) of the BRB, obtained from the tests. The 2nd and 3rd specimens —having an almost constant cross-section area in the yielding lateral bands of the core (see Fig. 5) and gaps fitted to the proposed value given by Eq. (1)— exhibited an almost identical response. Their compressive curves showed no waving from beginning to end. The P- δ curve of the 1st specimen, its gaps nearly doubling the proposed value given by Eq. (1), showed rippling in compression after its first plastic incursion (Fig. 8f), and increasing compressive forces in repetitive loops. The 4th specimen, with a lower gap than the values proposed in Eq. (1), increased its compressive load in repetitive amplitude loops (Fig. 8d) from the early stages onward. Yet unlike the 1st specimen, the P- δ curve of the 4th specimen in compression was quite smooth; rippling appeared at the last part of the test, when the compression force picked up, leading to local buckling failure (Fig. 8e).

The BRB has two sources of energy dissipation: (1) the plastic deformation of the yielding core and (2) the friction mechanism between the core and the restrainers. As for the second one, it is very important to keep the friction forces under control because it has implications not only for the ultimate energy dissipation capacity of the BRB but also for the shape of the hysteretic loops. Keeping the friction forces under control means (i) to limit the truss forces exerted by the waved yielding lateral bands against the restrainers, and

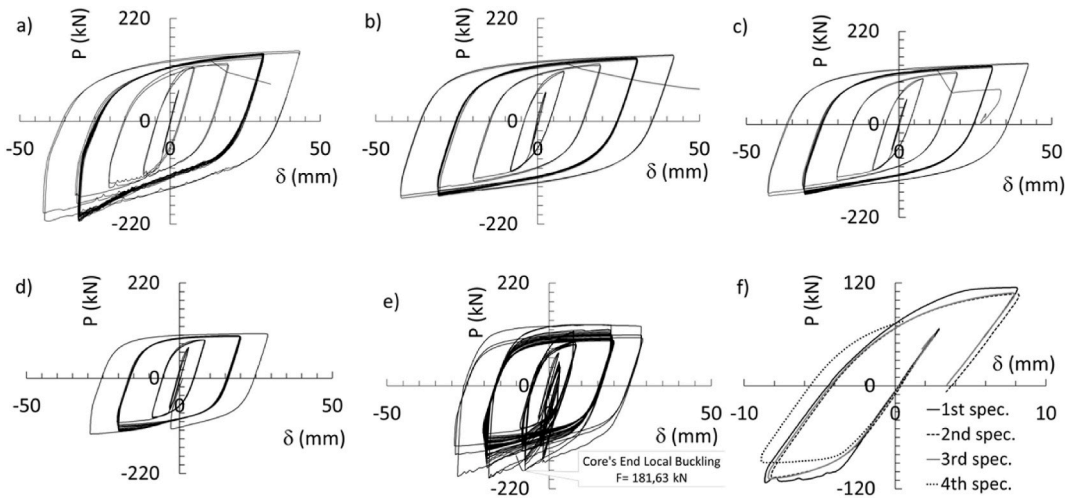

Fig. 8. Load-deformation hysteretic curves: a) 1st specimen; b) 2nd specimen; c) 3rd specimen; d) 4th specimen, first set of cycles; e) 4th specimen; f) first yielding cycle comparison.

(ii) to avoid the degradation of the contact surface between the yielding lateral bands and the restrainers because it raises the friction coefficient. To limit the truss forces it is necessary to ensure that the gaps between the core and the restrainers are regular and tightly adjusted to the required values. A certain gap is always mandatory to allow the expansion of the cross section of the lateral yielding bands in compression due to Poisson effect. A detailed examination of the hysteretic behavior of the 2nd and 3rd specimens (Fig. 8b and c) reveals that the shape of the loops is very regular and basically the same under tension and compression. This means that the BRB has a very stable hysteretic behavior. Further, the post yield stiffness is only about 1.5% of the elastic stiffness. This is a beneficial feature because it means that the BRB can dissipate energy without increasing significantly the forces imparted to the rest of the structure. Moreover, the fact that the shape of the loops is very close to a rectangle indicates an excellent ability to dissipate energy. The highly satisfactory hysteretic behavior and energy dissipation capacity exhibited by the 2nd and 3rd specimens were accomplished because the gaps fitted to the proposed values and the friction forces were well controlled. In contrast to the 2nd and 3rd specimens, the 1st specimen which gap was larger than the proposed value, developed higher amplitude waves and larger friction forces that turned out in a much lower energy dissipation capacity and different shapes of the hysteretic loops under tension and under compression forces (Fig. 8a).

Fig. 9 depicts the partial axial displacements measured at the lowermost and uppermost parts of the yielding lateral bands of the 2nd, 3rd and 4th specimens, as measured by displacement transducers DT-2 and DT-3. The 2nd specimen showed a balanced distribution of deformation. In contrast, the 3rd specimen, which was a twin of the 2nd, exhibited a clear unbalance —most probably due to the reuse of the ER. The 4th specimen also showed a pronounced unbalance, attributed to the fact that the cross-sectional area at the lowermost part of the yielding lateral bands was larger than in the rest of the core, as seen in Fig. 5. The unbalance of the 4th specimen took place before the third set of cycles of imposed deformations. In the last set of cycles, the trend was inverted, but both ends of the

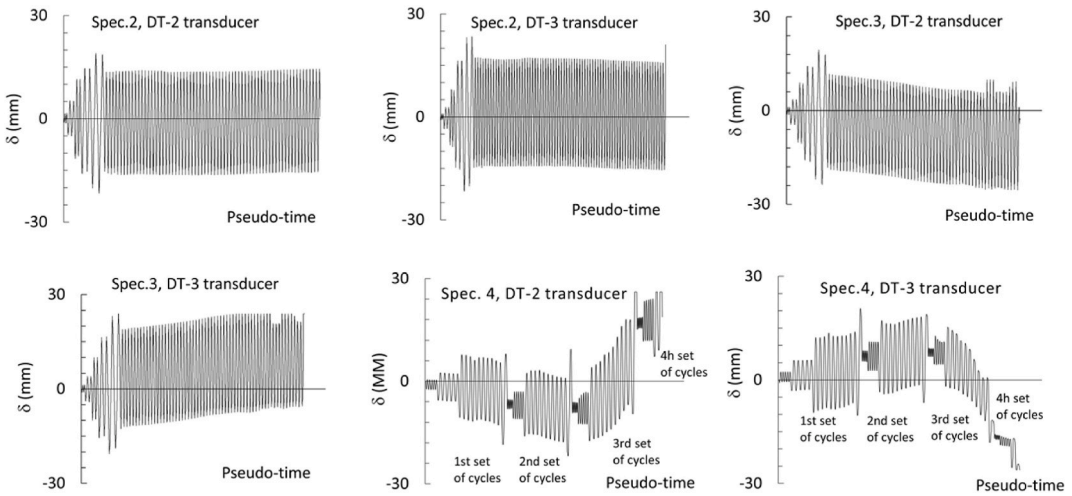

Fig. 9. Time-history deformation at both sides of the stoppers on specimens 2nd, 3rd and 4th.

yielding lateral bands remained totally operative. The uppermost part of the yielding lateral bands accumulated a significant amount of negative deformation and eventually got stuck in the IR due to the insufficient size of the gap g_z. Once the uppermost part of the yielding lateral bands was stuck, all deformation accumulated at the lowermost part of the yielding lateral bands. This led to peak compression forces and to local buckling failure, as discussed in the next sub-section.

Table 4 summarizes the relevant response parameters of the CDC-BRBs obtained in the tests. The values of some are predicted with the formulae proposed in Annexes A, B and C. Accordingly, P_y and δ_y are the axial yielding force and axial displacement at yielding; K_e is the axial elastic stiffness; β is the ratio of maximum axial compression strength to maximum tension strength; C_m and T_m are the maximum axial compression and maximum axial tension strength; $\delta_{c,e}$ is ultimate cumulative deformation; $\delta_{c,p}$ is the ultimate plastic cumulative deformation; δ_m is the maximum deformation, and ε_c its corresponding strain when normalized by L_y; δ_a is the maximum deformation amplitude on the yielding core (measured by transducer DT-1) and ε_a its corresponding strain when normalized by L_y; δ_{mh} is the maximum elongation in a half core at peak elongation amplitude, E_h is the total dissipated energy; μ, μ_a and μ_c are, respectively, the ratios of δ_m, δ_a, $\delta_{c,p}$ to the yielding deformation δ_y; and η is the normalized dissipated energy, defined as the ratio of energy dissipation E_h to the product $\delta_y P_y$. E_h was obtained by integrating the axial force-displacement curves, P-δ, obtained from the tests up to failure. Failure was assumed to occur when the applied force P began to decrease steadily under increasing forced displacements, as done in previous studies [22]. In case of specimen 4, failure was due to the local buckling of the unrestrained end parts of the core. In the calculation of μ, μ_a, μ_c and η, the predicted values of δ_y and P_y are used.

In view of the results displayed in Table 4, the following assertions can be made. First, irrespective of the dimension of the gap, P_y, δ_y and K_e can be well predicted with the formulae of Annex A. Second, if the dimension of the gaps is equal to or larger than the proposed values given by Eq. (1) (1st, 2nd and 3rd specimens), the β-factor can be well predicted with the formulae of Annex C. To the contrary, gaps less than the values proposed with Eq. (1) may lead part of the yielding lateral bands of the core to stick to the restrainers, meaning the loss of part of their functional length. This results in uncontrolled increments of the maximum compression force C_m and of the ratio β, which could reach an unforeseeable value, much greater than the one predicted with Eq. (C.1). Such is the case of the 4th specimen, exhibiting a value of β 35% larger than anticipated. Uncontrolled increments of β, and consequently of C_m, can cause local or global buckling of the BRB, or impart forces much larger than expected to the frame where the BRB is installed. Third, if the size of the gaps fits the proposed values of Eq. (1) (2nd and 3rd specimens), the low-cycle fatigue life of the CDC-BRB in terms of normalized accumulated plastic deformation μ_c or normalized total dissipated energy η can be reasonably well predicted with the formulae of Annex B. Contrariwise, having lower or larger gaps (1st and 4th specimens) leads to premature failure and a dramatic reduction of the energy dissipation capacity of the CDC-BRB. In the case of the 1st and 4th specimens, the values of μ_c and η were around 17% of that theoretically expected.

Table 5 shows the distribution of residual strains, after failure, across the yielding core. The residual strains were calculated at several cross-sections, plotted in Fig. 10. At each cross-section, we measured the thickness and width of the yielding lateral bands before testing and after failure to respectively obtain the corresponding total areas of cores A_c and A_{cf}. Then, from A_c and A_{cf}, assuming a Poisson coefficient $\nu = 0.5$ and neglecting second order deformation components, we estimated the residual strain ε_R as $\varepsilon_R=(A_c\text{-}A_{cf})/A_c$. In all specimens, the outer zones of the yielding lateral bands showed residual negative strains, while the inner zones showed positive residual strains. This pattern of residual strains was also reported in previous studies [8]. If the gaps fit the values proposed with Eq. (1) (2nd and 3rd specimens), the residual negative strains remain below 4%. Otherwise, having gaps that are larger (1st specimen) or smaller (4th specimen) than the values given by Eq. (1) would dramatically increase the residual negative strains —up to about 15%. In the 4th specimen the increase was particularly high (18.3%), as part of the core became stuck in the restrainer.

3.3.2. Local buckling of the unrestrained end parts of the core

The end portion of the core of the 4th specimen experienced local buckling at 181.63 kN of the compression load (see Fig. 8e). Buckling was followed by a significant lateral displacement of the ER as shown in Fig. 11a. An attempt was made to predict the buckling force $P_{cr,uc}$ with Euler's equation given by:

$$P_{cr,uc} = \pi^2 \frac{EI_{cz}}{(\alpha L_{uc})^2} \tag{8}$$

where E is Young's modulus, I_{cz} is the weak-axis moment of inertia at the core cross-section, L_{uc} is the unrestrained length of the end portion of the core, and α the column effective length factor, which depends on the end boundary conditions. The experimental value of L_{uc} was measured after the occurrence of the local buckling, giving 176.2 mm. Solving Eq. (8) setting either $P_{cr,uc}$ and L_{uc} into their experimental values, and considering $E = 2E{+}5$ MPa, the length factor becomes $\alpha = 1.98$. Therefore, it can be concluded that the force that triggers the local buckling of the unrestrained end portion of the core can be well predicted with Euler's Eq. (8) assuming free-clamped (i.e. $\alpha = 2$) boundary conditions (Fig. 11b). This is consistent with the fact that the gap-to-gussets and the hole-to-pin tolerance allow enough free rotation, as shown in Fig. 11a. The double hinge mechanism followed (as shown in Fig. 11a) as soon as the core contacted the gusset, because of the increasing lateral displacement of the ER.

It is of paramount importance to avoid the local buckling of the unrestrained end parts of the core since it jeopardises the response of the CDC-BRB. Thus, it shall be verified that the buckling force $P_{cr,uc}$ calculated with Eq. (8) is larger than the maximum force that can be endured by the yielding lateral bands of the CDC-BRB P_{Ed} given by Eq. (A.4). To this end, it is recommended to reduce the unrestrained length of the end portion of the core L_{uc} as much as possible.

Table 4
Experimental and theoretical response parameters.

	Test/prediction	Units	1st spec	2nd spec	3rd spec	4th spec
P_y	Test	kN	107	101	102	89
	Eq. (A.1)	kN	111.9	103.4	103.7	93.8
δ_y	Test	mm	3.9	3.5	3.5	3.1
	Eq. (A.6)	mm	3.92	3.58	3.58	3.22
K_e	Test	kN/mm	27.44	28.86	29.14	28.71
	Eq. (A.5)	kN/mm	25.73	25.98	26.06	26.23
T_m	Test	kN	150.2	142.6	144.5	131.1
C_m	Test	kN	214.7	164.0	169.0	197.3
β	Test	–	1.43	1.15	1.17	1.50
	Eq. (C.1)[a]	–	1.54	1.18	1.18	1.11
$\delta_{c,e}$	Test	mm	4020	9907	8210	3822
$\delta_{c,p}$	Test	mm	3456	8704	7208	2857
δ_m	Test	mm	43.92	42.27	42.96	58.02
$\varepsilon_c = \delta_m/L_y$	Test	%	1.63%	1.56%	1.59%	1.08%
δ_a	Test	mm	85.29	84.39	85.86	57.98
$\varepsilon_a = \delta_a/L_y$	Test	%	3.16%	3.12%	3.18%	2.15%
δ_{mh}	Test	mm	–	23.41	23.84	20.40
$\xi = 4\delta_{mh}/\delta_a$	Test	–	–	1.11	1.11	1.41
E_h	Test	kJ	386.4	930	781	289.2
$\mu = \delta_m/\delta_y$	Test	–	11.21	11.81	12.00	18.04
$\mu_a = \delta_a/\delta_y$	Test	–	21.77	23.57	23.98	18.03
$\mu_c = \delta_{c,p}/\delta_y$	Test	–	882	2431	2013	889
	Eq. (B.1)	–	3825	3325	3226	5330
$\eta = E_h/P_y\delta_y$	Test	–	881	2513	2104	959
	Eq. (B2)	–	4167	3702	3608	5515

[a] A friction factor of 0.1 was considered [4,18].

Table 5
Residual elongation ε_R related to Fig. 8 locations.

Specimen	1	2	3	4	5	6	7	8	9	10
1st	−8.47%	−1.93%	0.24%	−0.59%	5.04%	1.75%	0.24%	−2.57%	−4.03%	−4.54%
2nd	−1.61%	−0.87%	3.89%	4.84%	2.15%	7.16%	2.76%	4.75%	0.81%	−3.20%
3rd	−3.68%	−2.90%	2.09%	3.52%	3.50%	6.36%	6.22%	4.11%	2.82%	−3.00%
4th	−15.19%	−7.76%	1.00%	9.03%	10.23%	8.67%	8.07%	3.87%	−3.93%	−18.34%

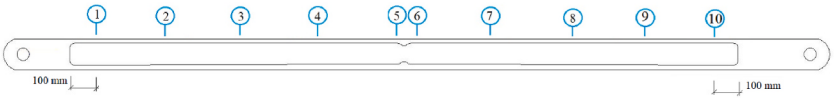

Fig. 10. Fixed locations to evaluate the residual elongation.

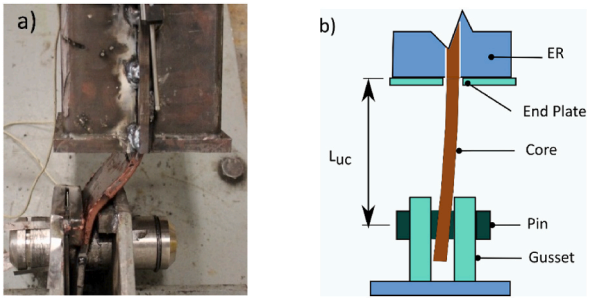

Fig. 11. Local buckling failure of the end portion of the core: a) 4th specimen's failure; b) ending core ideal buckling mode.

4. Conclusions

This papers proposes a new all-steel buckling restrained brace (BRB) named Coplanar Dual Core BRB (CDC-BRB) made up of three parts: the core, the restrainers, and a pin. The core consists of two lateral bands that are forced to yield under axially applied deformations (yielding lateral bands) whose buckling is prevented by an external restrainer (ER) and by an internal restrainer (IR). The

pin keeps the ER and the IR centered on the core; and if pulled out, it allows for core extraction for inspection/repair. The ER is composed of two rectangular tubes with end plates, welded at both (opposite) sides of two calibrated rectangular bars that control the size of the out-of-plane gap g_Y. Preferably, the core and the IR would be CAD-CAM laser cut from a single sheet of steel, preserving micro-connectors between the IR and the yielding lateral bands to improve their cross-section uniformity and control the size of the in-plane gap g_Z during the assemblage of the CDC-BRB. Formulae are provided here for the design of the CDC-BRB and for the prediction of the hysteretic response and ultimate energy dissipation capacity. More precisely, this study proposes formulae to determine the required size of the gaps g_Y, g_Z, and a simple elastic model to predict the deflection δ_w of the walls of the tubes that form the ER. In turn, δ_w is a key parameter to predict the maximum compression to tension strength ratio (β-factor) of the BRB. Four specimens of the new CDC-BRB were built and tested under cyclic loadings until failure to investigate the hysteretic response, so as to clarify the influence of the size of the gaps as well as validate the proposed formulae. The key difference among the specimens was the dimension of the gaps g_Y and g_Z. Moreover, the effect of repairing the CDC-BRB by replacing the core and the IR, and reusing the ER, was investigated. In the 1st specimen, the size of the gaps g_Y and g_Z exceeded the proposed values. The 2nd and 3rd specimens had the proposed gaps, the difference between them being the use of a new ER (2nd) or a reused one (3rd specimen). The 3rd specimen had gaps smaller than the proposed value. The following conclusions are put forth:

1. The specimens (2nd and 3rd) with the proposed gaps showed an almost identical hysteretic response in terms of axial force versus overall axial displacement. This means that repairing the CDC-BRB by substituting the core and the IR and reusing the ER does not affect the hysteretic curves. Notwithstanding, the reuse of the ER caused minor unbalance in terms of the partial axial displacements measured at the lowermost and uppermost parts of the yielding lateral bands.
2. The specimen (1st) with gaps larger than the proposed values, and the specimen with gaps smaller than proposed (4th), both increased the maximum compressive forces in repetitive hysteretic loops.
3. The specimen (4th) with gaps smaller than the required values accumulated a significant amount of negative deformation at the lowermost part of the yielding lateral bands, and eventually got stuck in the IR. This caused a shap rise in the compression force that triggered the local buckling failure of the unrestrained end part of the core. The local buckling force can be well predicted with Euler's equations using an effective length factor of 2 (i.e. free-clamped boundary conditions).
4. The dimensions of the gaps g_Y, g_Z do not affect the yield force P_y, the yield displacement δ_y, nor the elastic stiffness K_e of the CDC-BRB. If the gaps g_Y, g_Z are made equal to or larger than the proposed values, the maximum compression force C_m, and the ratio of maximum compression to tension force β, can be well predicted with the proposed formulae.
5. To predict β it is necessary to estimate the deflection δ_w of the walls of the tubes that form the ER due to the outward forces exerted by the yielding lateral bands in compression. A simple linear elastic model is put forth to calculate δ_w. The β predicted with this δ_w is very close to the test results.
6. If the size of the gaps is less than the proposed values, the yielding lateral bands of the core stick to the restrainers, resulting in large uncontrolled increments of the maximum compression force C_m (about 40%) and of the ratioβ (about 50%) that cannot be predicted.
7. If the size of the gaps fits the proposed values, the low-cycle fatigue life of the CDC-BRB in terms of normalized accumulated plastic deformation μ_c or normalized total dissipated energy η can be well predicted with the proposed formulae. On the contrary, gaps lower or larger than the proposed values cause premature failure of the CDC-BRB and significantly reduce (by 1/4 or more) its energy dissipation capacity in terms of normalized accumulated plastic deformation μ_c or normalized total dissipated energy.

Declaration of competing interest

The authors declare that they have no known competing financial interests or personal relationships that could have appeared to influence the work reported in this paper.

Data availability

Data will be made available on request.

Acknowledgements

We thank the company Oxiterri SL (Porqueres – Spain) for their patience and aid in improving the core's manufacturing process. The University of Girona (UdG) and AMADE research group (UdG) collaborated on testing the specimens. This work has been supported by the Spanish Government under Project MEC_PID2020-120135RB-I00 and received funds from the European Union (Fonds Européen de Dévelopment Régional).

ANNEX ADESIGN OF THE CDC-BRB

The CDC-BRB basic design expressions are the ones ordinarily used in BRBs:

$$P_y = F_y A_c \tag{A.1}$$

$$T_m = \omega P_y \tag{A.2}$$

$$C_m = \omega\beta P_y \tag{A.3}$$

where F_y is the specified minimum yielding stress, A_c is the total cross-sectional area of the lateral bands, P_y is the yielding strength, T_m and C_m are the maximum brace strengths at tension and compression, respectively, and the ratios ω and β are experimentally determined [17]. The connections of the BRB and all its components, other than the yielding lateral bands, must be designed for a factored maximum force P_{Ed} in order to guarantee that they remain elastic under the maximum forces endured by the yielding lateral bands. P_{Ed} [17] is given by:

$$P_{Ed} = R_y\, C_m \tag{A.4}$$

where R_y is the ratio of the expected yield stress to the specified minimum yield stress F_y of the steel. To estimate the elastic stiffness of the BRB, it is considered that the core is composed of two parts with constant cross-section. One part is the two yielding lateral bands of length L_{lb} and cross-sectional area A_c (see Fig. 2c). The other would be the solid zones at each end of the core of total length $L_e = L_b$-L_{lb}, and cross-sectional area $A_e = h \times t$. The meaning of variables L_b, L_{lb}, h and t that define the geometry of the BRB are shown in Fig. 2. E is the Young modulus of the steel of the core. Given these considerations, the elastic stiffness of the CDC-BRB is:

$$K_e = \frac{EA_cA_e}{A_eL_{lb} + A_cL_e} \tag{A.5}$$

When predicting the deformation at the yielding point we would consider the length of the lateral bands with uniform cross-sectional area, L_y:

$$\delta_y = \frac{P_yL_y}{A_cE} \tag{A.6}$$

According to EN-1993-1-8 [23], the bearing resistance, $F_{b,Rd}$, and the shear resistance $F_{v,Rd}$, of the pin connections located at each end of the CDC-BRB are:

$$F_{b,Rd} = \frac{1.5\; t\; d_e F_y}{\gamma_{M0}} \tag{A.7}$$

$$F_{v,Rd} = \frac{1.2\; A_p F_{u,p}}{\gamma_{M2}} \tag{A.8}$$

where d_e is the diameter of the pin, t is the core thickness (see Fig. 2c), A_p is the cross-sectional area of the pin, F_y and $F_{ub,p}$ are the yield stress and the ultimate stress, respectively, of the core steel and pin steel of the connection, and γ_{M0} (=1.0) and γ_{M2} (=1.25) are partial resistance factors given in Ref. [24]. As the ultimate stress of the pin's steel will be much higher than the yielding stress of the core's steel, and the pin will sustain double shear, the bearing resistance will establish the resistance of the joint. Then, considering $F_{b,Rd} \geq C_m$, together with Eqs. A.1, A.3 and A.4, the minimum pin diameter must satisfy:

$$d_e \geq \frac{4}{3}\beta\omega b \tag{A.9}$$

where b is the width of the yielding lateral bands (see Fig. 2).

The ER must guarantee the global stability of the SC-BR. For the sake of simplicity, it is assumed that the end portions of the core beyond the yielding lateral bands are rigid, and plastic hinges develop at either end of each yielding lateral band (see Fig. 3b). Under these simplifications, the eccentricities $e_{g,Y}$ and $e_{g,Z}$ of the axial force along the Y and Z axes (see Fig. 2) due to the gaps g_Y and g_z are:

$$e_{g,Z} = g_Z\frac{C}{C - C_0 - \xi\delta_{Ed}} - \frac{g_Z}{2}\;\;;\;\; e_{g,Y} = g_Y\frac{C}{C - C_0 - \xi\delta_{Ed}} - \frac{g_Y}{2} \tag{A.10}$$

where δ_{Ed} is the design elongation of the BRB. Substituting Eq. (4) in Eq. (A.10) gives:

$$e_{g,Y} = \frac{3}{2}g_Y\;\;;\;\; e_{g,Z} = \frac{3}{2}g_Z \tag{A.11}$$

To this end, the eccentricities given by Eq. (A.11) must be increased by the initial out-of-straightness imperfection of the ER in the Y and Z directions, $e_{0,Y}$ and $e_{0,Z}$. The ER must be designed to resist the combined action of the bending moments $M_{Ed,Y}$ and $M_{Ed,Z}$ produced by the design axial force of the core P_{Ed} and the eccentricities $(e_{g,zY} + e_{0,Y})$, $(e_{g,Z} + e_{0,Z})$, by satisfying the following condition at mid-cross section of the ER:

$$\frac{M_{Ed,Y}}{W_{el,Y}F_{yd,ER}} + \frac{M_{Ed,Z}}{W_{el,Z}F_{yd,ER}} \leq 1 \tag{A.12}$$

where:

$$M_{Ed,Y} = \frac{\mathrm{P_{Ed}}\left(\mathrm{e_{g,Z}} + \mathrm{e_{o,Z}}\right)}{1 - \mathrm{P_{Ed}}/\mathrm{P_{cr,Y}}} \;\; ; \;\; M_{Ed,Z} = \frac{P_{Ed}\left(e_{g,Z+}e_{o,Y}\right)}{1 - P_{Ed}/P_{cr,Z}} \tag{A.13}$$

Here, $F_{yd,ER}$ is the design yield strength of the steel used for the ER; $W_{el,y}$ and $W_{el,z}$ designate the elastic section modulus of the ER; and $P_{cr,Y}$, $P_{cr,Z}$ are Euler's buckling load in each direction given by:

$$P_{cr,Y} = \pi^2 \frac{\mathrm{EI_Y}}{\mathrm{L_b^2}} \;\; ; \;\; \mathrm{P_{cr,Z}} = \pi^2 \frac{EI_Z}{L_b^2} \tag{A.14}$$

Here, I_Y and I_Z are the moments of inertia of the ER along the Y and Z axes, while L_b is shown in Fig. 2b.

ANNEX BPREDICTION OF LOW-CYCLE FATIGUE LIFE

Tsai et al. experimentally demonstrated that there is a potential relationship between the cumulative plastic deformation and the maximum plastic strain on BRBs [10]. Based on this finding, the authors developed, in past research [8], the following formulae to predict the low-cycle fatigue of the BRB in terms of the cumulative plastic deformation coefficient μ_c, and the energy dissipation capacity coefficient η:

$$\mu_c = X\mu_a^{-\xi} \tag{B.1}$$

$$\eta = Z\mu_a^{-\zeta} \tag{B.2}$$

where $\mu_c = \delta_{c,p}/\delta_y$, $\mu_a = \delta_a/\delta_y$, $\eta = E_h/(\delta_y P_y)$, $\delta_{c,p}$ is the ultimate plastic cumulative deformation, δ_a is the maximum deformation amplitude of the CDC-BRB, δ_y as defined by Eq. (A.6), P_y as defined by Eq. (A.1), E_h is the hysteretic energy dissipated by the CDC-BRB, and X, ξ, Z and ζ are experimentally correlated coefficients whose proposed values are X = 868,161, $\xi = 1.761$, Z = 407,860, and $\zeta = 1.488$.

ANNEX C. PREDICTION OF β−FACTOR

The β-factor portrays how symmetric the hysteretic response is, and the effect of friction forces on the maximum compressive force of the BRB. β can be determined through the following expression [11]:

$$\beta = \frac{1 + |\varepsilon_c|}{1 - |\varepsilon_c|}\left(1 + 4c_f c_Y \frac{L_y}{L_{w,y}^2}\right) \tag{C.1}$$

where c_f is the frictional coefficient and c_Y is the functional gap between the core and the walls of the ER measured along the Y direction (see Fig. 2b). c_Y plays an important role when it comes to determining the β-factor, as it governs the amplitude of the high-mode buckling wave of the yielding lateral bands of the core and thus controls the friction forces produced by the core's outward forces in the Y direction. For the CDB-BRB, c_Y can be estimated considering the constructional gap g_Y, the corresponding deflection of the ER, δ_w, and the core's transversal expansion by the following expression:

$$c_Y = g_Y + \delta_w - |\varepsilon_c|\upsilon t \tag{C.2}$$

where ε_c is the maximum compressive strain given by (7), g_Y is given by Eq. (1), υ is the Poisson coefficient that can be taken as $\upsilon = 0.5$ in plastic behavior, and δ_w can be estimated with the simple linear elastic model proposed next. Consider a portion of the wall of one of the tubes that form the ER, deforming and waving according to the core's lateral band wavelength, L_{wy}, which can be computed with Eq. (6) by using the core thickness t instead of b. The model is based on a double symmetrical response (Fig. B1), according to which the width and the length of the plate are considered as one half of the wavelength L_{wy} and one half of the depth of the tube h_t, respectively. The edge of the plate adjacent to the folded wall is restrained against movements and rotations along the local X, Y and Z axes. The other edges of the model have symmetry constraints. Finally, it is considered that the plate is subjected to an outward force f_y distributed on an area having a width that is a third of the wavelength as well as a depth equal to the lateral bands' width b. The value of this outward force is taken as [4,8]:

$$f_y = 2P_{Ed}\frac{c_Y}{L_{wy}} \tag{C.3}$$

The plated model and the formerly described process were applied to estimate the β-factor of the tested specimens. The β-factor and functional gap g_y were determined from the described process, by means of Eq. (C.1) and Eq. (C.2), respectively, and a friction factor $c_f = 0.1$ [4,18], by an iterative process. Table C.1 offers the values of several parameters required to run the model plus the predictive equations and the obtained results, showing that β-factor prediction is satisfactory for the 1st, 2nd and 3rd specimens, whose gaps were larger than or equal to the values proposed with Eq. (1). Yet the prediction was not satisfactory for the 4th specimen, whose gap was smaller than the proposed value, because the yielding lateral bands got stuck in the ER. Results also show that when the gaps fit Eq. (1) values, the wall's deflection δ_w had a minor effect on the functional gap and β-factor, which could be determined directly from the constructional gap c_y.

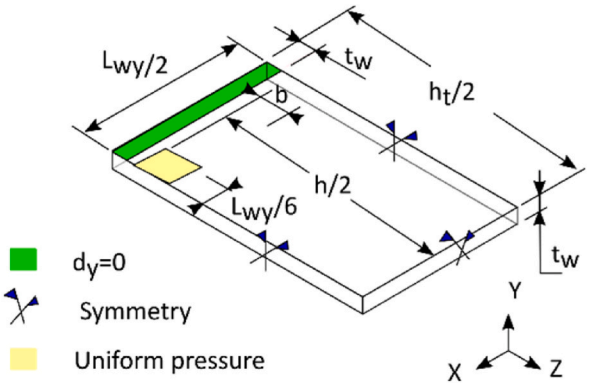

Fig. B1. Proposed model to estimate the deflection of the ER δ_w

Table C.1
Theoretical values of the functional gap c_Y and the β-factor for the tested specimens

	B (mm)	t_w (mm)	h_t (mm)	H (mm)	g_y (mm)	ε_a (%)	ε_c [b] (%)	L_{wy} (mm)	f_y [a] (kN)	δ_w [c] (mm)	c_y [g] (mm)	β_{est} [h]	β [i]	$(\beta_{est}$ - $\beta)/\beta_{est}$ (%)
	Test	Test	Test	Test	Test	Test	Test	Eq. (6)	Eq. (C3)	FEM	Eq. (C2)	Eq. (C1)	Eq. (C1)	
sp1	19,6	9.84	160	137.5	2.0	3.16%	1.580%	74.9	18.561	0.618	2.540	1.433	1.539	1.72%
sp2	19.5	10	160	137.5	0.7	3.12%	1.560%	76.8	4.036	0.142	0.764	1.167	1.178	0.16%
sp3	19.56	10	160	137.5	0.7	3.18%	1.590%	75.9	4.117	0.144	0.765	1.171	1.182	0.17%
sp4	19.7	10	160	137.5	0,7	2.15%	1.075%	97.1	1.894	0.061	0.707	1.108	1.108	−0.02%

[a] $\omega \approx \omega'$ (see table 2) to estimate P_{Ed}
[b] $\varepsilon_c \approx \varepsilon_a/2$
[c] δ_w was numerically obtained in the center of the loading area in the proposed model (Fig. B1).
[g] From Eq. (C2) and a 2nd iteration.
[h] From Eq. (C1) considering $c_Y = g_Y$
[i] From Eq. (C1) and a 2nd iteration.

References

[1] L. Dunai, Type Testing of Buckling-Restrained Braces According to EN 15129, 2011. Budapest.
[2] S. Merritt, C.-M. Uang, G. Benzoni, Subassemblage Testing of COREBRACE Buckling-Restrained Braces, La Jolla, California, 2003.
[3] C. Black, N. Makris, I. Aiken, Component testing, stability analysis and characterization of buckling-restrained Unbonded Braces, PEER Rep (2002/08 2002) 115.
[4] C.C. Chou, S.Y. Chen, Subassemblage tests and finite element analyses of sandwiched buckling-restrained braces, Eng. Struct. 32 (2010) 2108–2121, https://doi.org/10.1016/j.engstruct.2010.03.014.
[5] An-Chien, P.-C.L. Wu, K-Ct, High-mode buckling responses of buckling-restrained brace core plates, Earthq. Eng. Struct. Dynam. 43 (2013) 375–393, https://doi.org/10.1002/eqe.2349.
[6] R. Tremblay, P. Bolduc, R. Neville, R. DeVall, Seismic tests of thin buckling-restrained braces, Can. J. Civ. Eng. 33 (2006) 183–198.
[7] P.C. Lin, K.C. Tsai, Y.Y. Hsiao, A.C. Wu, Seismic tests of thin-profile buckling-restrained braces, in: NCEE 2014 - 10th U.S. Natl. Conf. Earthq. Eng. Front. Earthq. Eng., 2014, https://doi.org/10.4231/D37940V3K. Anchorage, Alaska.
[8] X. Cahís, E. Simon, D. Piedrafita, A. Catalan, Core behavior and low-cycle fatigue estimation of the perforated core buckling-restrained brace, Eng. Struct. (2018).
[9] G. Palazzo, F. López-Almansa, X. Cahís, F. Crisafulli, A low-tech dissipative buckling restrained brace. Design, analysis, production and testing, Eng. Struct. 31 (2009) 2152–2161, https://doi.org/10.1016/j.engstruct.2009.03.015.
[10] K. Tsai, J. Lai, Y. Hwang, Research and Application of Double-Core Buckling Restrained Braces in Taiwan, in: 13th World Conf. Earthq. Eng., 2004. Canada, Vancouver, B.C.
[11] Keh-Chyuan Tsai, An-Chien Wu, Chih-Yu Wei, Pao-Chun, M.-C.C. Lin, Y-Jy, Welded end-slot connection and debonding layers for buckling-restrained braces, Earthq. Eng. Struct. Dynam. 43 (2014) 1785–1807, https://doi.org/10.1002/eqe.2423.
[12] M. Iwata, M. Murai, Buckling-restrained brace using steel mortar planks; performance evaluation as a hysteretic damper, Earthq. Eng. Struct. Dynam. 35 (2006) 1807–1826, https://doi.org/10.1002/eqe.608.
[13] M.E. Eryasar, C. Topkaya, An experimental study on steel-encased buckling-restrained brace hysteretic dampers, Earthq. Eng. Struct. Dynam. (2010), https://doi.org/10.1002/eqe.959.
[14] T. Usami, C. Wang, J. Funayama, Low-cycle fatigue tests of a type of buckling restrained braces, Procedia Eng. 14 (2011) 956–964, https://doi.org/10.1016/j.proeng.2011.07.120.
[15] R. Tremblay, P. Bolduc, R. Neville, R. DeVall, Seismic testing and performance of buckling-restrained bracing systems, Can. J. Civ. Eng. (2006), https://doi.org/10.1139/l05-103.
[16] D. Piedrafita, X. Cahis, E. Simon, J. Comas, A new perforated core buckling restrained brace, Eng. Struct. 85 (2015) 118–126, https://doi.org/10.1016/j.engstruct.2014.12.020.
[17] American Institute of Steel Construction, ANSI/AISC 341-16. Seismic provisions for structural steel buildings, Seism Provisions Struct Steel Build 430 (2016) 111.
[18] N. Hoveidae, B. Rafezy, Overall buckling behavior of all-steel buckling restrained braces, J. Constr. Steel Res. 79 (2012) 151–158, https://doi.org/10.1016/j.jcsr.2012.07.022.

[19] (CEN) EC for S, BS EN ISO 6892-1:2016 Metallic Materi, 2016, https://doi.org/10.3403/30268532 als. Tensile testing. Method of test at room temperature.
[20] (CEN) EC for S. EN 10025 - 2 : 2004 Technical Delivery Conditions for Non-alloy Structural Steels 2004..
[21] Comité Européen de Normalisation (Cen), EN 15129. Antiseismic devices, Management (2009) 1–140.
[22] A. Benavent-Climent, A brace-type seismic damper based on yielding the walls of hollow structural sections, Eng. Struct. 32 (2010) 1113–1122.
[23] European Committee for Standarization, BS EN 1993-1-8:2005 - eurocode 3: design of steel structures - Part 1-8: design of joints, Eurocode 3 8 (2005) 135.
[24] (CEN) EC for S, Eurocode 3: design of steel structures - Part 1-1, General rules and rules for buildings 1 (2005).